



A numerical study of velocity-pressure gradient and pressure-dilatation terms in transport equations for subfilter turbulent kinetic energy in

Downloaded from: <https://research.chalmers.se>, 2026-05-14 15:54 UTC

Citation for the original published paper (version of record):

Lipatnikov, A., Sabelnikov, V. (2025). A numerical study of velocity-pressure gradient and pressure-dilatation terms in transport equations for subfilter turbulent kinetic energy in premixed flames. *Physics of Fluids*, 37(10). <http://dx.doi.org/10.1063/5.0294306>

N.B. When citing this work, cite the original published paper.

RESEARCH ARTICLE | OCTOBER 27 2025

A numerical study of velocity-pressure gradient and pressure-dilatation terms in transport equations for subfilter turbulent kinetic energy in premixed flames

Andrei N. Lipatnikov  ; Vladimir A. Sabelnikov 



Physics of Fluids 37, 105163 (2025)

<https://doi.org/10.1063/5.0294306>



Articles You May Be Interested In

A priori assessment of gradient models of joint cumulants for large eddy simulations of premixed turbulent flames

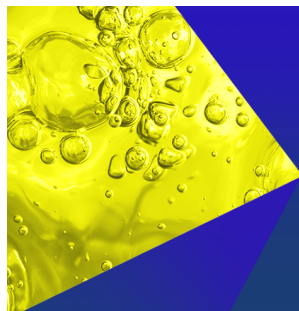
Physics of Fluids (July 2025)

Numerical errors in the computation of subfilter scalar variance in large eddy simulations

Physics of Fluids (May 2009)

An *a priori* analysis of the structure of local subfilter-scale species surrounding flame fronts using direct numerical simulation of turbulent premixed flames

Physics of Fluids (April 2021)



Physics of Fluids
Special Topics
Open for Submissions

[Learn More](#)

A numerical study of velocity-pressure gradient and pressure-dilatation terms in transport equations for subfilter turbulent kinetic energy in premixed flames

Cite as: Phys. Fluids **37**, 105163 (2025); doi: [10.1063/5.0294306](https://doi.org/10.1063/5.0294306)

Submitted: 2 August 2025 · Accepted: 13 October 2025 ·

Published Online: 27 October 2025



View Online



Export Citation



CrossMark

Andrei N. Lipatnikov^{1,a)} and Vladimir A. Sabelnikov²

AFFILIATIONS

¹Department of Mechanics and Maritime Sciences, Chalmers University of Technology, Gothenburg SE-412 96, Sweden

²ONERA - The French Aerospace Lab., F-91761 Palaiseau, France

^{a)}Author to whom correspondence should be addressed: lipatn@chalmers.se

ABSTRACT

Pressure-dilatation and velocity-pressure-gradient terms in transport equations for subfilter turbulent kinetic energy are *a priori* explored by analyzing published three-dimensional direct numerical simulation (DNS) data obtained from a lean (the equivalence ratio $\Phi = 0.81$) complex-chemistry hydrogen-air flame propagating in a box. The DNS conditions are associated with moderately intense (Kolmogorov time-scale is shorter than flame timescale by a factor of above two), small-scale (Kolmogorov length scale is smaller than laminar flame thickness by a factor of about 20) turbulence. The studied terms are computed by filtering out the DNS fields of velocity, pressure, and fuel mass fraction and adopting top hat filters of different widths, which are smaller or comparable with the laminar flame thickness. Moreover, gradient models of the second-order generalized central moments (joint cumulants) are extended to close the explored pressure terms. Reported results show that filtered pressure terms conditioned to filtered combustion progress variable change their sign with variations in the sampling variable. Moreover, magnitudes of the conditioned terms are much higher than magnitudes of the counterpart time- and transverse-averaged terms. In addition, spatial variations of time- and transverse averaged velocity-pressure-gradient or pressure-dilatation term within mean flame brush are well predicted by the newly introduced gradient models in all studied cases. While the sole model constant tuned to get the best prediction increases gradually with filter width, the constant remains of unity order in all cases. These results encourage further assessment of gradient models as a promising tool for large eddy simulation of premixed turbulent combustion.

© 2025 Author(s). All article content, except where otherwise noted, is licensed under a Creative Commons Attribution (CC BY) license (<https://creativecommons.org/licenses/by/4.0/>). <https://doi.org/10.1063/5.0294306>

I. INTRODUCTION

Large eddy simulations (LES) of turbulent flows^{1–4} are widely used to directly resolve motion of large-scale eddies by separating them from small-scale ones. For this purpose, unsteady three-dimensional fields $f(\mathbf{x}, t)$ are filtered out over sufficiently small volumes

$$\bar{f}(\mathbf{x}, t) = \int G(\mathbf{x}, \xi, \Delta) f(\xi, t) d^3 \xi, \quad (1)$$

where $G(\mathbf{x}, \xi, \Delta)$ is a generic filter kernel in space

$$\int G(\mathbf{x}, \xi, \Delta) d^3 \xi = 1, \quad (2)$$

and the filter width Δ characterizes the wavelength of the smallest scale retained by the filtering operation. When running LES of compressible non-reacting flows⁴ and flames,^{5–9} the Favre-filtered fields $\tilde{f} = \overline{\rho f} / \bar{\rho}$ are commonly considered for the mass conservation equation

$$\frac{\partial \bar{\rho}}{\partial t} + \frac{\partial}{\partial x_j} (\bar{\rho} \tilde{u}_j) = 0, \quad (3)$$

to involve resolved terms only. Here, t and x_j are the time and Cartesian coordinates, ρ is the density, u_i is i -th components of the velocity vector \mathbf{u} , and the Einstein summation convention applies to repeated indexes.

Favre-filtered Navier–Stokes Equation reads

$$\frac{\partial}{\partial t}(\overline{\rho\tilde{u}_i}) + \frac{\partial}{\partial x_j}(\overline{\rho\tilde{u}_j\tilde{u}_i}) = -\frac{\partial}{\partial x_j}(\overline{\rho\tilde{\tau}_{ij}}) - \frac{\partial\overline{p}}{\partial x_i} + \frac{\partial\overline{\tau_{\mu,ij}}}{\partial x_j}, \quad (4)$$

where \overline{p} designates the filtered pressure, $\tilde{\tau}_{ij} = \widetilde{u_i u_j} - \tilde{u}_i \tilde{u}_j$ and $\overline{\tau_{\mu,ij}}$ are the subfilter-scale (SFS) stress tensor and the viscous tensor, respectively, with μ referring to molecular dynamic viscosity. In the simplest case of single-step-chemistry, adiabatic burning, and equal molecular diffusivities of major reactants, the following transport equation:

$$\frac{\partial}{\partial t}(\overline{\rho\tilde{c}}) + \frac{\partial}{\partial x_j}(\overline{\rho\tilde{u}_j\tilde{c}}) = -\frac{\partial\overline{\tilde{F}_j}}{\partial x_j} + \frac{\partial\overline{J}_j}{\partial x_j} + \overline{\omega}_c, \quad (5)$$

for the Favre-filtered combustion progress variable \tilde{c} is widely used.⁵⁻⁹ Here, $\overline{\omega}_c$ designates the filtered mass rate of product creation, $\overline{\tilde{F}_j} = \overline{\rho(\tilde{u}_j\tilde{c} - \tilde{u}_j\tilde{c})}$ and \overline{J}_j are SFS and molecular diffusion fluxes, respectively. In this simplest case, mixture state is characterized with a single scalar c , which monotonically increases from zero in unburned reactants to unity in equilibrium adiabatic combustion products,

Most terms on the right-hand sides of Eqs. (4) and (5) are unresolved, with various models^{6,8-18} of the rate $\overline{\omega}_c$ involving the SFS turbulent kinetic energy $k_{sfs} = (\widetilde{u_i u_i} - \tilde{u}_i \tilde{u}_i)/2$. Within the LES framework, the evolution of this energy is often simulated using a transport equation, which can be written in different forms, e.g.

$$\begin{aligned} & \frac{\partial}{\partial t}(\overline{\rho\tilde{k}_{sfs}}) + \frac{\partial}{\partial x_i}(\overline{\rho\tilde{u}_i\tilde{k}_{sfs}}) + \frac{\partial}{\partial x_i} \left\{ \left[\frac{\widetilde{u_i u_i^2}}{2} - \frac{\tilde{u}_i \tilde{u}_i^2}{2} - \tilde{u}_j \widetilde{u_i u_j} + \tilde{u}_i \tilde{u}_j^2 \right] \right. \\ & \quad \left. - \overline{u_j \tau_{\mu,ij}} + \overline{u_j \tilde{\tau}_{\mu,ij}} + \overline{p u_i} - \overline{p u_i} \right\} \\ & = -\overline{\rho\tilde{\tau}_{ij}} \frac{\partial\tilde{u}_j}{\partial x_i} + (\tilde{u}_i - \overline{u}_i) \frac{\partial\overline{p}}{\partial x_i} + \overline{p} \frac{\partial\tilde{u}_i}{\partial x_i} - \overline{p} \frac{\partial\tilde{u}_i}{\partial x_i} \\ & \quad - (\tilde{u}_j - \overline{u}_j) \frac{\partial\overline{\tau_{\mu,ij}}}{\partial x_i} - \overline{\tau_{\mu,ij}} \frac{\partial\tilde{u}_j}{\partial x_i} + \overline{\tau_{\mu,ij}} \frac{\partial\tilde{u}_j}{\partial x_i} \end{aligned} \quad (6)$$

or

$$\begin{aligned} & \frac{\partial}{\partial t}(\overline{\rho\tilde{k}_{sfs}}) + \frac{\partial}{\partial x_i}(\overline{\rho\tilde{u}_i\tilde{k}_{sfs}}) \\ & \quad + \frac{\partial}{\partial x_i} \left[\overline{p} \left(\frac{\widetilde{u_i u_i^2}}{2} - \frac{\tilde{u}_i \tilde{u}_i^2}{2} - \tilde{u}_j \widetilde{u_i u_j} + \tilde{u}_i \tilde{u}_j^2 \right) \right] \\ & = -\overline{\rho\tilde{\tau}_{ij}} \frac{\partial\tilde{u}_j}{\partial x_i} + (\tilde{u}_i - \overline{u}_i) \frac{\partial\overline{p}}{\partial x_i} - \overline{u_i} \frac{\partial\overline{p}}{\partial x_i} + \overline{u}_i \frac{\partial\overline{p}}{\partial x_i} \\ & \quad - (\tilde{u}_j - \overline{u}_j) \frac{\partial\overline{\tau_{\mu,ij}}}{\partial x_i} + \overline{u_j} \frac{\partial\overline{\tau_{\mu,ij}}}{\partial x_i} - \overline{u_j} \frac{\partial\overline{\tau_{\mu,ij}}}{\partial x_i}. \end{aligned} \quad (7)$$

Since

$$\frac{\partial}{\partial x_i}(-\overline{u_j \sigma_{ij}} + \overline{u_j \tilde{\sigma}_{ij}}) = -\overline{\sigma_{ij}} \frac{\partial\tilde{u}_j}{\partial x_i} + \overline{\tilde{\sigma}_{ij}} \frac{\partial\tilde{u}_j}{\partial x_i} - \overline{u_j} \frac{\partial\overline{\sigma_{ij}}}{\partial x_i} + \overline{u_j} \frac{\partial\overline{\tilde{\sigma}_{ij}}}{\partial x_i}, \quad (8)$$

Equations (6) and (7) are mathematically identical. The sole difference between them consists in either splitting terms that involve the stress tensor $\sigma_{ij} = \tau_{\mu,ij} - p\delta_{ij}$ into a transport term and a source/sink term, i.e., $\partial(u_j \sigma_{ij})/\partial x_i$ and $\sigma_{ij} \partial u_j / \partial x_i$ on the left- and right-hand sides of Eq. (6), respectively (lhs and rhs, respectively), or using the single term $u_j \partial \sigma_{ij} / \partial x_i$ on the rhs of Eq. (7). Here, δ_{ij} is Kronecker delta. In

combustion literature, the former and latter approaches, i.e., the use of terms that involve either dilatation or pressure gradient, respectively, were adopted, e.g., in Refs. 9,19 and,²⁰⁻²³ respectively. Modeling of such pressure terms is an important unresolved issue, because they are known to play a crucial role in balance of turbulent kinetic energy within premixed flames.^{9,24-26} Accordingly, the issue is addressed in the present work.

Note that the pressure terms in Eqs. (6) and (7) are sometimes combined with the second term on the rhs of Eq. (6) or (7), as will be discussed later. Moreover, these terms can be rewritten as follows:

$$\overline{p} \frac{\partial\tilde{u}_i}{\partial x_i} - \overline{p} \frac{\partial\tilde{u}_i}{\partial x_i} = \overline{\tau}(p, \Theta), \quad (9)$$

where $\Theta \equiv \nabla \cdot \mathbf{u}$ designates dilatation, and

$$-\overline{u_i} \frac{\partial\overline{p}}{\partial x_i} + \overline{u_i} \frac{\partial\overline{p}}{\partial x_i} = -\overline{\tau}\left(u_i, \frac{\partial p}{\partial x_i}\right), \quad (10)$$

within framework of the second-order generalized central moments^{27,28} (joint cumulants)

$$\overline{\tau}(f, g) \equiv \overline{fg} - \overline{f}\overline{g}, \quad (11)$$

of two fields $f(\mathbf{x}, t)$ and $g(\mathbf{x}, t)$. Other joint cumulants are widely used in LES research into various turbulent flows. Specifically, the SFS stress tensor $\widetilde{u_i u_j} - \tilde{u}_i \tilde{u}_j$, the SFS scalar flux $\widetilde{u_i c} - \tilde{u}_i \tilde{c}$, the SFS scalar variance $\overline{c^2} - \overline{c}^2$, and the velocity difference $\tilde{u}_i - \overline{u}_i$, which is multiplied with the mean pressure gradient on the rhs of Eq. (6) or (7), are examples of joint cumulants $\overline{\tau}(u_i, u_j)$, $\overline{\tau}(u_i, c)$, $\overline{\tau}(c, c)$, and $\overline{\tau}(\rho, u_i)/\overline{\rho}$, respectively.

All these joint cumulants require closure relations. Such relations can be yielded by so-called gradient models put forward by Leonard²⁹ and by Clark *et al.*³⁰ by developing pioneering ideas of Smagorinsky,³¹ who introduced a scalar subfilter-scale viscosity. Gradient models are also of eddy-viscosity type but introduce a subfilter-scale viscosity tensor. Capabilities of such models for predicting the cumulants $\overline{\tau}(u_i, u_j)$, $\overline{\tau}(u_i, c)$, and $\overline{\tau}(c, c)$ in premixed flames were already demonstrated.^{9,32-37} Here

$$\overline{\tau}(f, g) \equiv \overline{fg} - \overline{f}\overline{g}, \quad (12)$$

is a counterpart of the cumulant $\overline{\tau}(f, g)$ within Favre-averaging framework. Recently, predictive capabilities of gradient models for five such cumulants, i.e., $\overline{\tau}(u_i, u_j)$, $\overline{\tau}(u_i, c)$, $\overline{\tau}(c, c)$, $\overline{\tau}(\rho, u_i)$, and $\overline{\tau}(\rho, c) = \overline{\rho c} - \overline{\rho}\overline{c}$ were shown³⁸ by analyzing the same (for all cumulants) Direct Numerical Simulation (DNS) data. However, to the best of the present authors' knowledge, the pressure-containing cumulants $\overline{\tau}(p, \Theta)$ and $\overline{\tau}(\mathbf{u}, \nabla p)$ have not yet been addressed in combustion literature.

Accordingly, the goal of the present work is twofold: (i) a study of the behavior of the joint cumulants $\overline{\tau}(p, \Theta)$ and $\overline{\tau}(\mathbf{u}, \nabla p)$ in a premixed turbulent flame and (ii) *a priori* assessment of the performance of gradient models for these two terms. For these purposes, direct numerical simulation (DNS) data created by Dave *et al.*³⁹ and Dave and Chaudhuri⁴⁰ are analyzed. Note that the same DNS data were recently used³⁸ to validate gradient models for five other joint cumulants, i.e., $\overline{\tau}(u_i, u_j)$, $\overline{\tau}(u_i, c)$, $\overline{\tau}(c, c)$, $\overline{\tau}(\rho, u_i)$, and $\overline{\tau}(\rho, c)$.

Gradient models of $\overline{\tau}(p, \Theta)$ and $\overline{\tau}(\mathbf{u}, \nabla p)$ are introduced in the next section. In the third section, the DNS attributes are reported.

Computed results are presented and discussed in the fourth section, followed by conclusions.

II. GRADIENT MODELS

As already noted, gradient models were pioneered by Leonard²⁹ and by Clark *et al.*³⁰ for incompressible flows. Later, the approach was extended and applied to other problems^{2,41–58} such as compressible turbulence, mixing and heat transfer, reacting flows, etc. Here, following studies by Liu *et al.*,⁴¹ by Cimarelli *et al.*,⁵⁷ and by Berselli *et al.*,⁵⁸ gradient model equations are obtained by (i) applying Taylor expansion to a similarity model by Bardina *et al.*,⁵⁹ which was originally proposed for incompressible flows, and (ii) considering the lowest-order terms.

The original similarity model by Bardina *et al.*⁵⁹ assumes that $u'_i = u_i - \bar{u}_i$ and $\bar{u}'_i = \bar{u}_i - \bar{u}_i$ are of the same order of magnitude. Subsequently, application of $u'_i \approx \bar{u}'_i$ to all terms in the Leonard triple decomposition for subfilter stresses $\bar{\tau}(u_i, u_j)$, i.e., the Leonard stresses (interactions between filtered scales), cross-stresses (interactions between filtered and subfiltered scales), and Reynolds subfilter stresses (interactions between subfilter scales), results in $\bar{\tau}(u_i, u_j) \approx \bar{\tau}(\bar{u}_i, \bar{u}_j)$. It should be noted that Leonard stresses and cross-stresses considered separately are not Galilean invariants, while their sum is. Therefore, the linear combination model by Bardina *et al.*,⁵⁹ in which the cross-stress term is multiplied with a constant different from unity is not Galilean invariant.⁶⁰

A version of the model by Bardina *et al.*⁵⁹ reads

$$\bar{\tau}(f, g) \approx \bar{\tau}(\bar{f}, \bar{g}) = \overline{\bar{f}\bar{g}} - \bar{f}\bar{g}, \quad (13)$$

and results in⁵⁷

$$\begin{aligned} \bar{\tau}(f, g) \approx & \frac{1}{2} \iint G(\mathbf{x}, \boldsymbol{\eta}) G(\mathbf{x}, \boldsymbol{\xi}) [\bar{f}(\boldsymbol{\xi}, t) - \bar{f}(\boldsymbol{\eta}, t)] \\ & \times [\bar{g}(\boldsymbol{\xi}, t) - \bar{g}(\boldsymbol{\eta}, t)] d^3 \boldsymbol{\xi} d^3 \boldsymbol{\eta}, \end{aligned} \quad (14)$$

because

$$\begin{aligned} \iint G(\mathbf{x}, \boldsymbol{\eta}) G(\mathbf{x}, \boldsymbol{\xi}) \bar{f}(\boldsymbol{\xi}, t) \bar{g}(\boldsymbol{\eta}, t) d^3 \boldsymbol{\xi} d^3 \boldsymbol{\eta} &= \overline{\bar{f}\bar{g}}, \\ \iint G(\mathbf{x}, \boldsymbol{\eta}) G(\mathbf{x}, \boldsymbol{\xi}) \bar{f}(\boldsymbol{\xi}, t) \bar{g}(\boldsymbol{\xi}, t) d^3 \boldsymbol{\xi} d^3 \boldsymbol{\eta} &= \overline{\bar{f}\bar{g}}. \end{aligned} \quad (15)$$

By applying the first-order Taylor expansion to the differences in the integral in Eq. (14), we arrive at

$$\begin{aligned} \bar{\tau}(f, g) \approx & \frac{\partial \bar{f}}{\partial x_j} \frac{\partial \bar{g}}{\partial x_k} \frac{1}{2} \iint G(\mathbf{x}, \boldsymbol{\eta}) G(\mathbf{x}, \boldsymbol{\xi}) (\xi_j - \eta_j) (\xi_k - \eta_k) d^3 \boldsymbol{\xi} d^3 \boldsymbol{\eta} \\ &= \tau(x_j, x_k) \frac{\partial \bar{f}}{\partial x_j} \frac{\partial \bar{g}}{\partial x_k}. \end{aligned} \quad (16)$$

For a regular Cartesian control volume and a top-hat filter of width Δ , i.e.

$$G_\Delta(\mathbf{x}, \boldsymbol{\xi}) = \frac{1}{\Delta^3} \left[1 - H\left(|\boldsymbol{\xi}| - \frac{\Delta}{2}\right) \right], \quad (17)$$

where H is Heaviside function, Eq. (16) reads

$$\bar{\tau}(f, g) \approx \frac{1}{12} \Delta^2 \frac{\partial \bar{f}}{\partial x_k} \frac{\partial \bar{g}}{\partial x_k}. \quad (18)$$

Substitution of various pairs of $\{f = p, g = \Theta\}$ or $\{f = \mathbf{u}, g = \nabla p\}$ into Eq. (18) yields

$$\bar{\tau}(p, \Theta) = \overline{p\Theta} - \bar{p}\bar{\Theta} = \frac{1}{12} \Delta^2 \frac{\partial \bar{p}}{\partial x_k} \frac{\partial \bar{\Theta}}{\partial x_k}, \quad (19)$$

or

$$\bar{\tau}(\mathbf{u}, \nabla p) = \overline{u_i \partial p} - \bar{u}_i \bar{\partial p} = \frac{1}{12} \Delta^2 \frac{\partial \bar{u}_i}{\partial x_k} \frac{\partial^2 \bar{p}}{\partial x_i \partial x_k}. \quad (20)$$

In Sec. IV, Eqs. (19) and (20) are assessed by analyzing DNS database created by Dave *et al.*³⁹ and Dave and Chaudhuri⁴⁰ described briefly in the next section.

III. DNS ATTRIBUTES AND DIAGNOSTIC METHODS

Since the DNS database was already discussed by the present authors in previous articles,^{38,61–68} only a summary of the DNS attributes is given below. The reader interested in further details is referred to the cited papers.

A statistically one-dimensional and planar, lean (the equivalence ratio $\Phi = 0.81$) hydrogen-air flame propagating in a cuboid ($19.18 \times 4.8 \times 4.8$ mm) was simulated using Pencil code⁶⁹ to numerically integrate unsteady and three-dimensional continuity, compressible Navier–Stokes, energy and species transport equations supplemented the ideal gas state equation. Moreover, a detailed chemical mechanism (9 species and 21 reactions) by Li *et al.*⁷⁰ and the mixture-averaged molecular transfer model were invoked.

The cuboid was meshed with a uniform grid of $960 \times 240 \times 240$ cells. Periodic and Navier–Stokes characteristic boundary conditions⁷¹ were set at the transverse sides and the inlet or outlet, respectively.

Homogeneous isotropic turbulence was generated in another cube adopting large-scale forcing³⁶ and setting the periodic boundary conditions. The turbulence evolved until a statistically stationary state was reached. At this stage,³⁹ the r.m.s. velocity $u' = 6.7$ m/s; an integral length scale $L = 3.1$ mm; the integral timescale $\tau_t = L/u' = 0.46$ ms; the turbulent Reynolds number $Re_t = u'L/\nu = 950$; the Kolmogorov length scale $\eta = (\nu^3/\langle \epsilon \rangle)^{1/4} = 0.018$ mm, and the Kolmogorov timescale $\tau_\eta = (\nu/\langle \epsilon \rangle)^{1/2} = 0.015$ ms. Here, ν designates kinematic viscosity; $\langle \epsilon \rangle = \langle 2\nu S_{ij} S_{ij} \rangle$ is the turbulence dissipation rate averaged over the cube; and $S_{ij} = (\partial u_i/\partial x_j + \partial u_j/\partial x_i)/2$ is the rate-of-strain tensor.

At $t = 0$, a laminar flame pre-computed using the same chemical mechanism and the same transport model was embedded into the cuboid at $x = x_0$. Under the simulation conditions (pressure $P = 1$ bar, and unburned gas temperature $T_u = 310$ K), the laminar flame speed S_L , thickness $\delta_L = (T_b - T_u)/\max\{|\nabla T|\}$, and timescale $\tau_f = \delta_L/S_L$ are equal to 1.84 m/s, 0.36 mm, and 0.20 ms, respectively. Here, subscripts u and b refer to unburned and burned mixtures, respectively. At $t > 0$, the flame was stretched by turbulence injected continuously into the computational domain through the left boundary $x = 0$. The Damköhler number $Da = (L/u')/(\delta_L/S_L)$ and the Karlovitz number $Ka^* = (u'/S_L)^{3/2} (L/\delta_L)^{-1/2}$ or $Ka = \tau_f/\tau_\eta$,

calculated using characteristics of the injected turbulence, are equal to 2.35 and 2.4 or 13, respectively.

Since the turbulence decayed along the x -direction, different turbulence characteristics were evaluated at the leading edge of the mean flame brush, i.e., were averaged over the plane $x = x_{le}(t)$ nearest to a cross section where the transverse-averaged combustion progress variable $\langle c \rangle(x, t) = 0.01$, followed by time-averaging. Specifically, $\overline{\langle u' \rangle}(x_{le}) = 3.3$ m/s; the Taylor length scale $\lambda(x_{le}) = \sqrt{15\nu_u \overline{\langle u' \rangle} / \overline{\langle \varepsilon \rangle}} = 0.25$ mm or $0.69\delta_L^T$; the Kolmogorov length scale $\eta(x_{le}) = 0.018$ mm or $0.05\delta_L^T$; the Kolmogorov timescale $\tau_\eta(x_{le}) = 0.087$ ms; the Reynolds number $Re_\lambda(x_{le}) = \overline{\langle u' \rangle} \lambda / \nu_u = 55$; and $Ka(x_{le}) = 2.3$ is much smaller than $(\delta_L / \eta)^2 \cong 400$, because $S_L \delta_L / \nu_u \gg 1$ in moderately lean hydrogen-air mixtures.⁷² Here, the combustion progress variable is defined using fuel mass fraction Y_F , i.e., $c = 1 - Y_F / Y_{F,u}$; symbol $\overline{\langle \cdot \rangle}$ refers to time- and transverse-averaged quantities sampled at 58 instants from $t = 1.0$ to $t = 1.57$ ms.

The density field $\rho(\mathbf{x}, t)$, the velocity field $\mathbf{u}(\mathbf{x}, t)$, and the combustion progress variable field $c(\mathbf{x}, t)$, obtained in the DNS, were filtered out using box (top-hat) filters, see Eq. (17), of different widths Δ , equal to $0.22\delta_L$, $0.44\delta_L$, and $0.88\delta_L$.

When testing Eqs. (19) and (20), the model constants b_D and b_G , respectively, were inserted into these equations, i.e., the following gradient model equations:

$$\overline{\tau}(p, \Theta) = \overline{p\Theta} - \overline{p}\overline{\Theta} = \frac{b_D}{12} \Delta^2 \frac{\partial \overline{p}}{\partial x_k} \frac{\partial \overline{\Theta}}{\partial x_k}, \quad (21)$$

and

$$\overline{\tau}(\mathbf{u}, \nabla p) = \overline{u_i \frac{\partial p}{\partial x_i}} - \overline{u_i} \frac{\partial \overline{p}}{\partial x_i} = \frac{b_G}{12} \Delta^2 \frac{\partial \overline{u_i}}{\partial x_k} \frac{\partial^2 \overline{p}}{\partial x_i \partial x_k}. \quad (22)$$

were assessed. Here, subscripts D and G in b_D and b_G refer to dilatation and gradient, respectively.

In the following, variations of the considered time- and transverse-averaged filtered terms, i.e., $\overline{\langle \tau(p, \Theta) \rangle}$ and $\overline{\langle \tau(\mathbf{u}, \nabla p) \rangle}$, within mean flame brush are reported vs time- and transverse-averaged combustion progress variable by taking advantage of the monotonic increase in $\langle c \rangle(x)$ from zero to unity with distance x . Moreover, the terms $\overline{\langle \tau(p, \Theta) | \bar{c} = \xi \rangle}$ and $\overline{\langle \tau(\mathbf{u}, \nabla p) | \bar{c} = \xi \rangle}$ conditioned to $|\bar{c}(\mathbf{x}, t) - \xi| < \Delta \xi$

with $\Delta \xi = 0.05$ and sampled from the entire flame brush over all instants will also be reported in the next section.

IV. RESULTS AND DISCUSSION

Figure 1 shows spatial variations of normalized (using $\delta_L / \rho_u S_L^3$) time- and transverse-averaged terms $\overline{\langle \tau(p, \Theta) \rangle}$ (red solid lines) and $\overline{\langle -\tau(\mathbf{u}, \nabla p) \rangle}$ (black dashed lines) along the normal to the mean flame brush. The latter term is taken with sign minus to be consistent with the rhs of Eq. (7). The same two terms are plotted in black dots in Fig. 2, where variations of the conditioned terms $\overline{\langle \tau(p, \Theta) | \bar{c} = \xi \rangle}$ and $\overline{\langle -\tau(\mathbf{u}, \nabla p) | \bar{c} = \xi \rangle}$ are presented in color lines. Since the following discussion of these conditioned terms is solely restricted to qualitative trends, Fig. 2 presents results sampled using a single filter of a medium width, i.e., $\Delta = 0.44\delta_L$. The following trends are worth noting.

First, magnitudes of the mean terms $\overline{\langle \tau(p, \Theta) \rangle}$ and $\overline{\langle -\tau(\mathbf{u}, \nabla p) \rangle}$ are increased with increasing the filter width Δ , cf. scales of ordinate axes in Figs. 1(a)–1(c). The same trend is observed for the conditioned terms $\overline{\langle \tau(p, \Theta) | \bar{c} = \xi \rangle}$ or $\overline{\langle -\tau(\mathbf{u}, \nabla p) | \bar{c} = \xi \rangle}$, but is not shown for brevity. This trend is associated with the fact that the small difference in $\overline{p\Theta}$ and $\overline{p}\overline{\Theta}$ or $\overline{\mathbf{u} \cdot \nabla p}$ and $\overline{\mathbf{u}} \cdot \nabla \overline{p}$ tends to zero as $\Delta \rightarrow 0$. On the contrary, magnitudes of the mean large subterms $\overline{p\Theta}$, $\overline{\mathbf{u} \cdot \nabla p}$, and $\overline{\mathbf{u}} \cdot \nabla \overline{p}$ depend weakly on Δ (see Fig. 3).

Note that the magnitudes of subterms $\overline{p\Theta}$ and $\overline{\mathbf{u} \cdot \nabla p}$ are significantly larger than the magnitudes of $\overline{\mathbf{u}} \cdot \nabla \overline{p}$ and $\overline{\mathbf{u}} \cdot \nabla \overline{p}$, cf. scales of ordinate axes in Figs. 3(a) and 3(b), respectively, whereas the magnitudes of the mean cumulants $\overline{\langle \tau(p, \Theta) \rangle}$ or $\overline{\langle -\tau(\mathbf{u}, \nabla p) \rangle}$ are comparable (see Fig. 1). Consequently, the former cumulant is a small difference between two large terms and, hence, is expected to be sensitive to numerical errors. From this perspective, the use of the latter cumulant, i.e., $\overline{\tau(\mathbf{u}, \nabla p)}$, could be preferable for numerical research into premixed turbulent combustion. This is a peculiarity of flames, where the filtered dilatation $\overline{\Theta}$ can attain significant values and, hence can yield a large term $\overline{p\Theta}$ after multiplication with the large filtered pressure \overline{p} . In iso-thermic flows characterized by a low Mach number, the filtered dilatation is small and the discussed sensitivity of $\overline{\tau}(p, \Theta)$ to numerical errors is expected to be weak. Accordingly, the cumulant $\overline{\tau}(p, \Theta)$ is widely used in LES research into non-reacting flows.^{28,73–75}

Second, magnitudes of terms plotted in Figs. 1 and 3 peak in the middle of the flame brush, because these magnitudes are increased with increasing probability of finding local flames (where dilatation

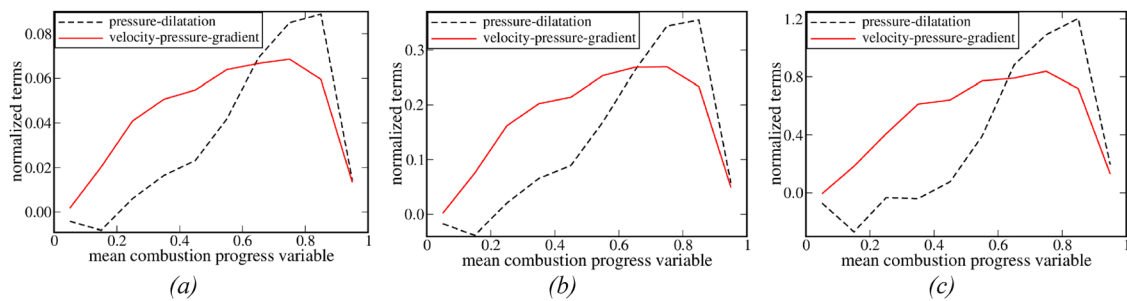


FIG. 1. Variations of time- and transverse-averaged terms $\overline{\langle \tau(p, \Theta) \rangle}$ (black dotted-dashed lines) and $\overline{\langle -\tau(\mathbf{u}, \nabla p) \rangle}$ (red solid lines) within mean flame brush. All terms are normalized using $\delta_L / (\rho_u S_L^3)$. (a) $\Delta = 0.22\delta_L$, (b) $\Delta = 0.44\delta_L$, and (c) $\Delta = 0.88\delta_L$.

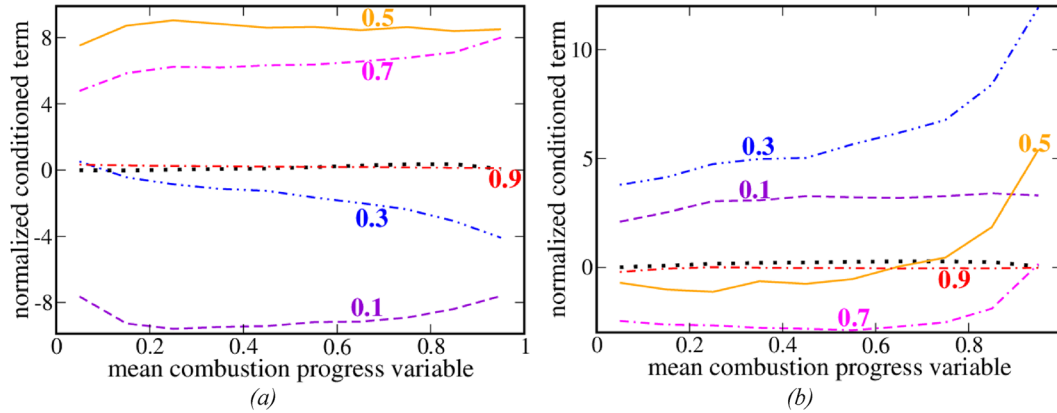


FIG. 2. Variations of (a) pressure-dilatation term $\bar{\tau}(p, \Theta)$ and (b) velocity-pressure-gradient term $\bar{\tau}(\mathbf{u}, \nabla p)$ within mean flame brush. Black dotted lines show time- and transverse-averaged terms $\langle \bar{\tau}(p, \Theta) \rangle$ and $\langle -\bar{\tau}(\mathbf{u}, \nabla p) \rangle$. Color lines show conditioned terms $\langle \bar{\tau}(p, \Theta) | \bar{c} = \xi \rangle$ and $\langle -\bar{\tau}(\mathbf{u}, \nabla p) | \bar{c} = \xi \rangle$, with the values of the conditioning variable ξ being specified near curves. All terms are normalized using $\delta_L / (\rho_u S_L^3)$. $\Delta = 0.44\delta_L$.

does not vanish and pressure gradient is high) and the latter probability is the largest in the middle of the flame brush. Since shapes of curves in Fig. 1 are controlled by the same physical mechanism (dependence of that probability on mean combustion progress variable), the shapes vary weakly with the filter width. Specifically, dependencies of $\langle \bar{\tau}(p, \Theta) \rangle$ or $\langle \bar{\tau}(\mathbf{u}, \nabla p) \rangle$ on $\langle \bar{c} \rangle$, sampled using $\Delta = 0.22\delta_L$ and $\Delta = 0.44\delta_L$, can be matched almost perfectly by multiplying the former (smaller filter width) dependencies with 3.96 and 3.94, respectively. A similar observation holds for $\Delta = 0.22\delta_L$ and $\Delta = 0.88\delta_L$, with matching coefficients being equal to 12.4 for $\langle \bar{\tau}(p, \Theta) \rangle$ and 11.8 for $\langle \bar{\tau}(\mathbf{u}, \nabla p) \rangle$. However, the matching is worse for $\Delta = 0.22\delta_L$ and $\Delta = 0.88\delta_L$ when compared to $\Delta = 0.22\delta_L$ and $\Delta = 0.44\delta_L$.

Third, Fig. 2 shows that the mean term magnitudes, see curves plotted in black dots, are much smaller than magnitudes of the conditioned terms sampled at $0.1 \leq \xi \leq 0.7$, see color lines. These differences in the magnitudes of $\langle \bar{\tau}(p, \Theta) \rangle$ and $\langle \bar{\tau}(p, \Theta) | \bar{c} = \xi \rangle$ or $\langle \bar{\tau}(\mathbf{u}, \nabla p) \rangle$ and $\langle \bar{\tau}(\mathbf{u}, \nabla p) | \bar{c} = \xi \rangle$ are associated with the fact that

velocity and pressure gradients are localized to thin zones in a typical premixed turbulent flame and, in particular, in the studied flame.⁶³ When averaging is performed over a transverse plane, probability of finding such zones is low and the mean terms $\bar{p}\Theta$ or $\bar{\mathbf{u}} \cdot \nabla \bar{p}$ and $\bar{\mathbf{u}} \cdot \nabla \bar{p}$ are relatively small. When averaging is solely performed over volumes where $\bar{c}(\mathbf{x}, t)$ is finite and varies weakly, e.g., $\bar{c}(\mathbf{x}, t) \approx \xi = 0.5$, probability of finding large dilatation or large pressure gradient is substantial and the magnitudes of the conditioned terms $\langle \bar{p}\Theta | \bar{c} = \xi \rangle$ and $\langle \bar{p}\Theta | \bar{c} = \xi \rangle$ or $\langle \bar{\mathbf{u}} \cdot \nabla \bar{p} | \bar{c} = \xi \rangle$ and $\langle \bar{\mathbf{u}} \cdot \nabla \bar{p} | \bar{c} = \xi \rangle$ are significantly larger when compared to their mean counterpart. Moreover, the discussed large differences in the magnitudes of $\langle \bar{\tau}(p, \Theta) \rangle$ and $\langle \bar{\tau}(p, \Theta) | \bar{c} = \xi \rangle$ or $\langle \bar{\tau}(\mathbf{u}, \nabla p) \rangle$ and $\langle \bar{\tau}(\mathbf{u}, \nabla p) | \bar{c} = \xi \rangle$ stem from cancelation of positive and negative contributions to the time- and transverse-averaged terms from the counterpart terms conditioned to various ξ .

Indeed, fourth, both magnitudes and signs of the conditioned terms depend on ξ (see Fig. 2). For instance, magnitudes of $\langle \bar{\tau}(p, \Theta) | \bar{c} = 0.1 \rangle$ and $\langle \bar{\tau}(p, \Theta) | \bar{c} = 0.5 \rangle$ are comparable, but their

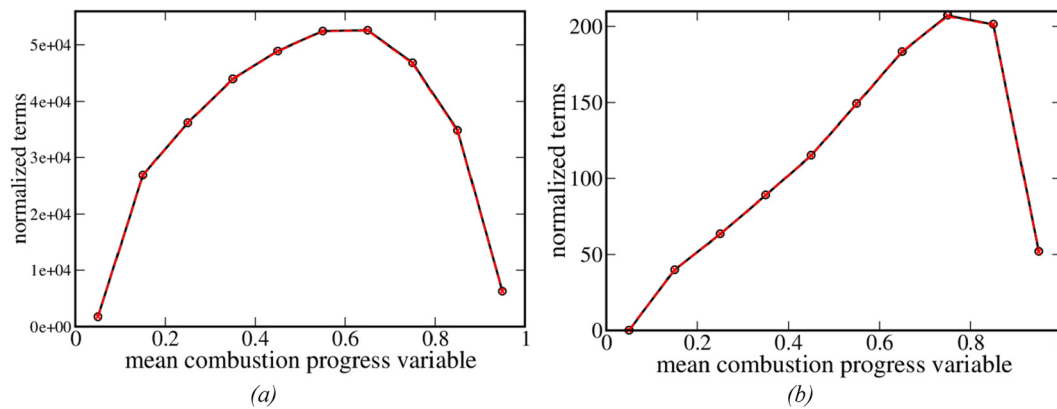


FIG. 3. Variations of time- and transverse-averaged terms (a) $\langle \bar{p}\Theta \rangle$ (lines) and $\langle \bar{p}\Theta \rangle$ (symbols) or (b) $-\langle \bar{\mathbf{u}} \cdot \nabla \bar{p} \rangle$ (lines) and $-\langle \bar{\mathbf{u}} \cdot \nabla \bar{p} \rangle$ (symbols) within mean flame brush. Black and red lines/symbols show results obtained using, $\Delta = 0.22\delta_L$ and $\Delta = 0.88\delta_L$, respectively. All terms are normalized using $\delta_L / (\rho_u S_L^3)$.

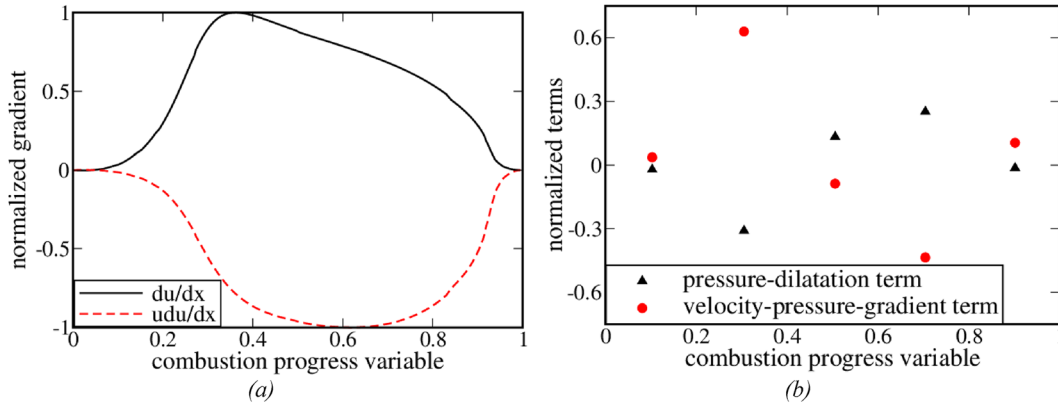


FIG. 4. (a) Dependencies of terms du/dx (black solid line) and udp/dx (red dashed line), normalized using their peak values, on combustion progress variable in the unperturbed laminar flame corresponding to DNS conditions. (b) Dependencies of terms $\bar{\tau}(p, \Theta)$ and $\bar{\tau}(\mathbf{u}, \nabla p)$ on combustion progress variable. The terms are filtered over the unperturbed laminar flame using $\Delta = 0.44\delta_L$ and normalized with $\delta_L/(\rho_u S_L^3)$.

signs are opposite, cf. curves plotted in violet dashed and orange solid lines, respectively, Fig. 2(a). Moreover, the term $\langle \bar{\tau}(\mathbf{u}, \nabla p) | \bar{c} = \xi \rangle$ has the largest magnitude and positive at $\xi = 0.3$, see curve plotted in blue double-dotted-dashed line in Fig. 2(b). Furthermore, the term $\langle \bar{\tau}(\mathbf{u}, \nabla p) | \bar{c} = \xi \rangle$ is negative at $\xi = 0.7$; see curve plotted in magenta dotted-double-dashed line in Fig. 2(b).

These trends can be understood by recalling that, in spite of $(\delta_L/\eta)^2 \cong 400$, the studied flame statistically retains the local structure of the counterpart unperturbed laminar premixed flame.^{61,62,64,65} In the latter flame, pressure monotonously decreases from unburned to burned sides, whereas dilatation grows from zero to a peak value reached at $c \approx 0.35$ and decreases with further increasing c , see curve plotted in black solid line in Fig. 4(a). Accordingly, correlation between pressure and dilatation should be negative and positive at $c < c^*$ and $c > c^*$, respectively, with $c^* \approx 0.35$. This simple reasoning explains the change of the signs of the term $\langle \bar{\tau}(p, \Theta) | c = \xi \rangle$ from negative to positive with increasing the sampling variable ξ [see Fig. 2(a)].

Furthermore, pressure gradient in a stationary, planar, one-dimensional laminar flame can be estimated as follows:⁷⁶ $dp/dx = -\rho u du/dx$ if viscous forces are neglected or $dp/dx = -\rho_u S_L du/dx = -\rho_u S_L \Theta$ due to the continuity equation $\rho u = \rho_u S_L$. Consequently,

in the laminar flame, $udp/dx = -0.5 \rho_u S_L du^2/dx$, i.e., spatial variations of udp/dx are solely controlled by $-du^2/dx$. The latter term is plotted in red dashed line in Fig. 4(a). In this simplest case, the velocity u monotonously increases from unburned to burned sides, whereas dilatation grows from zero to a peak value reached at $c^* \approx 0.35$ and decreases with further increasing c . Accordingly, correlation between u and $-dp/dx = \rho_u S_L \Theta$ should be positive and negative at $c < c^*$ and $c > c^*$, respectively. These simple reasoning explain the change of the signs of the term $\langle -\bar{\tau}(\mathbf{u}, \nabla p) | c = \xi \rangle$ from positive to negative with increasing the sampling variable ξ [see Fig. 2(b)].

To further support this explanation, the studied cumulants were filtered out over the unperturbed laminar flame. Results reported in Fig. 4(b) are fully consistent with the DNS data plotted in Fig. 2. In both cases, the pressure-dilatation cumulant is negative (positive) at small (large, respectively) c . On the contrary, the velocity-pressure-gradient cumulant is negative (positive) at large (small, respectively) c .

Dependencies of both sign and magnitude of $\langle \bar{\tau}(p, \Theta) | c = \xi \rangle$ or $\langle \bar{\tau}(\mathbf{u}, \nabla p) | \bar{c} = \xi \rangle$ on ξ could pose a challenge to models of $\bar{\tau}(p, \Theta)$ or $\bar{\tau}(\mathbf{u}, \nabla p)$ for LES of premixed turbulent combustion. Nevertheless, gradient models successfully address this challenge, as shown in Fig. 5,

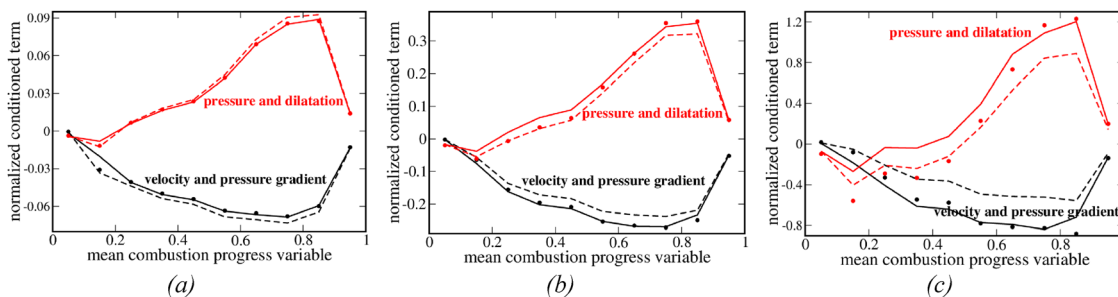


FIG. 5. Assessment of gradient models for subfilter pressure-dilatation term $\bar{\tau}(p, \Theta)$ (red lines or dots) and subfilter velocity-pressure-gradient term $\bar{\tau}(\mathbf{u}, \nabla p)$ (black lines or dots). Solid lines show time- and transverse-averaged terms $\langle \bar{\tau}(p, \Theta) \rangle$ and $\langle \bar{\tau}(\mathbf{u}, \nabla p) \rangle$ sampled directly from the DNS data. Dashed lines show results yielded straightforwardly by gradient models, see Eqs. (21) and (22) with the constants $b_D = b_G = 1$. Dots show the results yielded by gradient models with tuned values of the constants b_G and b_D , reported in Table I. All terms are normalized using $\delta_L/(\rho_u S_L^3)$. (a) $\Delta = 0.22\delta_L$. (b) $\Delta = 0.44\delta_L$. (c) $\Delta = 0.88\delta_L$.

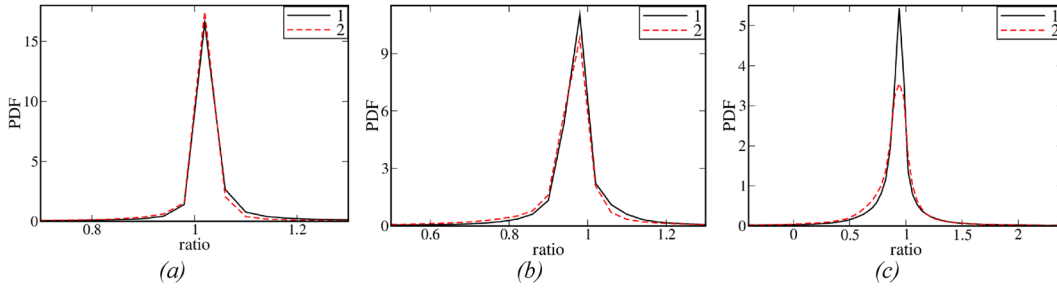


FIG. 6. Probability density functions for ratios of the filtered term $\bar{\tau}_{GM}$ yielded by gradient models to the counterpart filtered term $\bar{\tau}_{DNS}$ sampled directly from DNS data. $1-\bar{\tau}(\mathbf{u}, \nabla p)$ (black solid lines), $2-\bar{\tau}(p, \Theta)$ (red dashed lines). No tuning, i.e., the gradient-model constants $b_D = b_G = 1$ in Eqs. (21) and (22). (a) $\Delta = 0.22\delta_L$. (b) $\Delta = 0.44\delta_L$. (c) $\Delta = 0.88\delta_L$.

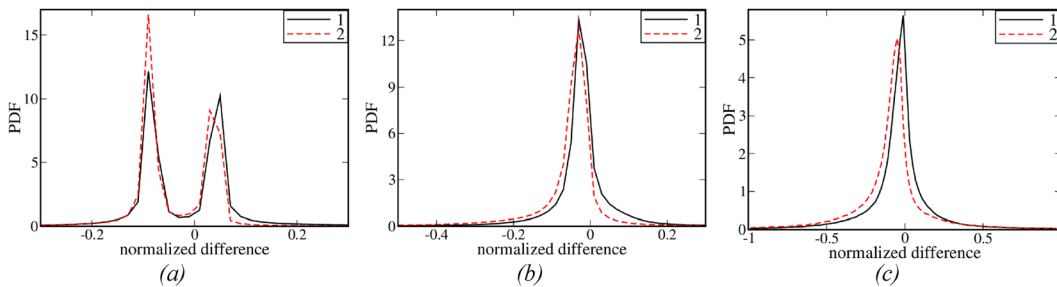


FIG. 7. Probability density functions for normalized differences ϵ calculated using Eq. (23). $1-\bar{\tau}(\mathbf{u}, \nabla p)$ (black solid lines), $2-\bar{\tau}(p, \Theta)$ (red dashed lines). No tuning, i.e., the gradient-model constants $b_D = b_G = 1$ in Eqs. (21)–(22). (a) $\Delta = 0.22\delta_L$. (b) $\Delta = 0.44\delta_L$. (c) $\Delta = 0.88\delta_L$.

TABLE I. Tuned values of model constants and differences between DNS data and model results.

$\Delta/\Delta x$	Equation (21)						Equation (22)					
	4	8	16	4	8	16	4	8	16	4	8	16
b	1	1	1	0.94	1.12	1.39	1	1	1	0.93	1.14	1.59
ϵ	0.06	0.13	0.29	0.04	0.08	0.24	0.19	0.13	0.33	0.15	0.06	0.19
δ	0.01	0.03	0.06	0.005	0.02	0.05	0.025	0.03	0.08	0.016	0.009	0.03

which reports results of assessing such models for both $\bar{\tau}(p, \Theta)$ and $\bar{\tau}(\mathbf{u}, \nabla p)$, see red and black lines, respectively. The DNS data (solid lines) are reasonably well predicted by Eqs. (21) and (22) with $b_D = b_G = 1$ (dashed lines).

In addition to the time- and transverse-averaged filtered cumulants addressed in Fig. 5, gradient models were also assessed for the local filtered cumulants. For this purpose, first, the ratio $r = \bar{\tau}_{GM}/\bar{\tau}_{DNS}$ of the filtered cumulants $\bar{\tau}_{GM}$ and $\bar{\tau}_{DNS}$, yielded by Eq. (21) or (22) and sampled from the DNS data, respectively, was locally evaluated. Second, the relative difference between these cumulants was locally computed as follows:

$$\epsilon = \frac{2(\bar{\tau}_{DNS} - \bar{\tau}_{GM})}{|\bar{\tau}_{DNS}| + |\bar{\tau}_{GM}|}. \quad (23)$$

Finally, probability density functions (PDF) for r and ϵ were sampled at $0.05 < \bar{c}(\mathbf{x}, t) < 0.95$ and $0.05 < \langle \bar{c}(\mathbf{x}, t) \rangle(x) < 0.95$. Obtained results are reported in Figs. 6 and 7, respectively, where black solid and red dashed lines refer to $\bar{\tau}(\mathbf{u}, \nabla p)$ and $\bar{\tau}(p, \Theta)$, respectively.

These figures show good performance of the gradient models for both cumulants on the local level. Specifically, the PDFs exhibit sufficiently narrow peaks at $r \approx 1$ and $\epsilon \approx 0$. It is of interest to note that the PDF for ϵ , sampled adopting the smallest filter, has two peaks at positive and negative ϵ [see Fig. 7(a)]. Specifically, the probabilities of finding $\epsilon \approx -0.1$ or $\epsilon \approx 0.05$ are significantly larger than the probability of finding much smaller $|\epsilon| \ll 1$. These apparently surprising trends (two peaks for $\Delta = 0.22\delta_L$ in Fig. 7(a), but a single peak for $\Delta = 0.44\delta_L$ or $\Delta = 0.88\delta_L$ in Figs. 7(b) or 7(c), respectively) could stem from (i) finite pointwise values of ϵ due to the neglected higher-order terms in Taylor expansion in Eq. (14), (ii) weak variations in these small values within a small volume ($\Delta = 0.22\delta_L$), but (iii) mutual cancelation of positive and negative small values of ϵ in different small parts of larger volumes ($\Delta = 0.44\delta_L$ or $\Delta = 0.88\delta_L$).

Despite generally good performance of these gradient models, Figs. 5–7 show their limitations also. For instance, differences in the mean $\langle \bar{\tau}_{GM} \rangle$ and $\langle \bar{\tau}_{DNS} \rangle$ are substantially larger at $\Delta = 0.88\delta_L$, see curves plotted in solid and dashed lines in Fig. 5(c). Moreover, an

increase in Δ results in substantially increasing the PDF width (see Figs. 6 and 7). Nevertheless, performance of Eqs. (21) and (22) can be improved by tuning the constants b_D and b_G , respectively, cf. curves plotted in solid lines and dots in Fig. 5. These results have been obtained by minimizing a difference of $\sum_{i=1}^N (\langle \tau_{DNS} \rangle_i - \langle \tau_{GM} \rangle_i)^2$ between time- and transverse-averaged joint cumulants $\langle \tau_{DNS} \rangle_i$ extracted directly from the DNS data and the counterpart cumulants $\langle \tau_{GM} \rangle_i$ yielded by the GM Eqs. (21) and (22). Here, $i = 1, \dots, N$ refers to various $\langle \bar{c} \rangle_i$ -bins. Since this simplest approach performs well, alternative methods were not tried.

Differences between the DNS data and results yielded by Eqs. (21) and (22) without ($b_D = b_G = 1$) or with adjusted constants are quantified adopting the following measures:

$$\epsilon = \frac{\max\left\{|\langle \tau_{DNS} \rangle_i - \langle \tau_{GM} \rangle_i|\right\}}{\max\left\{|\langle \tau_{DNS} \rangle_i|\right\}}; \quad (24)$$

$$\delta = \frac{\sqrt{\sum_{i=1}^N (\langle \tau_{DNS} \rangle_i - \langle \tau_{GM} \rangle_i)^2}}{N \max\left\{|\langle \tau_{DNS} \rangle_i|\right\}}. \quad (25)$$

Here, the maximum values are taken over various $\langle c \rangle_i$ -bins. Table I shows that both ϵ and, especially, δ are small.

The tuned values of b_D and b_G , reported in Table I and in Fig. 8, show a gradual increase with Δ . In LES applications, this trend could be addressed, e.g., by adopting a dynamic-modeling approach pioneered by Germano.^{28,77} Nevertheless, the tuned values remain of unity order and this fact implies that gradient models are promising even for the pressure-containing terms. However, it is worth noting that the largest filter width used in the present work is on the order of laminar flame thickness. Such a limitation is typical for *a priori* analysis of DNS data obtained from three-dimensional complex chemistry turbulent flames, because a ratio of computational width to δ_L is still rather moderate in such simulations reviewed elsewhere.⁷⁸ Nevertheless, close agreement between curves plotted in solid and dotted lines in Fig. 5 lends support to gradient models.

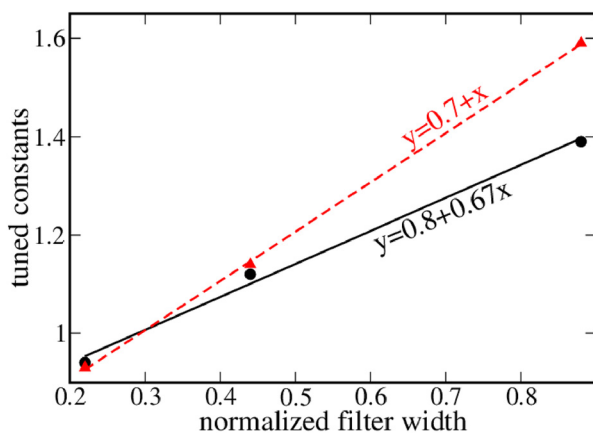


FIG. 8. Tuned values of constants in Eq. (21), black circles and solid line, and Eq. (22), red triangles and dashed line.

Recently, Wang *et al.*²³ tested the following equation:

$$\overline{u_i \frac{\partial p}{\partial x_i}} - \tilde{u}_i \frac{\partial \bar{p}}{\partial x_i} = C_p \Delta^2 \frac{\partial \tilde{u}_i}{\partial x_k} \frac{\partial^2 \bar{p}}{\partial x_i \partial x_k}, \quad (26)$$

in their *a priori* analysis of DNS data obtained from a premixed swirling flame. However, to get good agreement between Eq. (26) and those DNS data, Wang *et al.*²³ were forced to significantly increase C_p when compared to 1/12. On the face of it, these recent results appear to be inconsistent with the present analysis. However, this is not so, because the left-hand side of Eq. (26) differs from $\bar{\tau}(\mathbf{u}, \nabla p)$ analyzed by us. Indeed

$$\begin{aligned} \overline{u_i \frac{\partial p}{\partial x_i}} - \tilde{u}_i \frac{\partial \bar{p}}{\partial x_i} &= \overline{u_i \frac{\partial p}{\partial x_i}} - \bar{u}_i \frac{\partial \bar{p}}{\partial x_i} + (\bar{u}_i - \tilde{u}_i) \frac{\partial \bar{p}}{\partial x_i} \\ &= \bar{\tau} \left(u_i, \frac{\partial p}{\partial x_i} \right) + (\bar{u}_i - \tilde{u}_i) \frac{\partial \bar{p}}{\partial x_i}, \end{aligned} \quad (27)$$

i.e., the closure relation assessed by Wang *et al.*²³ differs from the gradient model explored by us, see Eq. (22). Note that the last term on the rhs of Eq. (27) describes baroclynal work, which stems from “strain generation by pressure and density gradients, both barotropic and baroclinic” and “can transfer energy across scales in variable density flows.”⁷⁹ Accordingly, the notion of baroclynal work is widely used in LES research into compressible turbulence.^{74,75} In premixed flames, this work also plays an important role, e.g., see a recent study,³⁸ where a gradient model of baroclynal work is validated against the DNS data by Dave *et al.*,³⁹ and Dave and Chaudhuri⁴⁰ analyzed in the present paper.

Finally, it is worth noting that certain *a posteriori* studies^{32,47,57} have shown that gradient models are numerically unstable. To resolve this problem, some modifications were suggested to numerically stabilize such models. Specifically, certain modifications rely on adopting some kind of “clipping”^{80–82} or combining a gradient model with an eddy viscosity model.^{30,83,84} The reader interested a detailed analysis of these approaches is referred to a recent paper by Cimarelli *et al.*⁵⁷ These issues are beyond the scope of the present paper but call for future *a posteriori* studies of gradient models in LES of premixed turbulent flames. Nevertheless, the good performance of such models shown in Figs. 5–7 and in our recent paper³⁸ appears to justify efforts aimed at solving the problem of numerical stability of gradient models.

V. CONCLUDING REMARKS

Pressure-dilatation and velocity-pressure-gradient terms in transport equations for subfilter turbulent kinetic energy were *a priori* explored by analyzing three-dimensional DNS data obtained by Dave *et al.*³⁹ and Dave and Chaudhuri⁴⁰ from a moderately lean complex-chemistry hydrogen-air flame propagating in moderately intense, small-scale turbulence in a box. The terms were computed by filtering out the DNS fields of velocity, pressure, and fuel mass fraction and adopting top hat filters of different widths, which were smaller or comparable with laminar flame thickness.

In addition, gradient models of the second-order generalized central moments (joint cumulants), which were mainly applied to subfilter turbulent stresses and scalar fluxes in various flows, were further extended to close the explored pressure terms.

The reported numerical results show that the filtered pressure terms conditioned to filtered combustion progress variable $\bar{c}(\mathbf{x}, t) = \xi$ change their sign with variations in the sampling variable ξ . These

changes were explained by analyzing laminar flame structure. In addition, magnitudes of the conditioned terms are much higher than magnitudes of the counterpart time- and transverse-averaged filtered pressure terms. Besides, the obtained results give priority to using the filtered velocity-pressure-gradient term when compared to the filtered pressure-dilatation term, because, in flames, the latter term is a small difference in two very large quantities and, therefore, can be more sensitive to numerical errors.

Moreover, spatial variations of time- and transverse averaged filtered pressure-dilatation and velocity-pressure-gradient terms within mean flame brush were shown to be well predicted by the newly introduced gradient models in all studied cases (different filter widths). While the sole model constant tuned to get the best prediction increases gradually with filter width, the constant remains of unity order in all cases. It is worth stressing, however, that quantitative results such as tuned values of the model constants are specific to the studied problem and require further investigation under substantially different conditions.

These results complement recent validation³⁸ of gradient models of five other filtered cumulants, i.e., $\bar{\tau}(u_i, u_j)$, $\bar{\tau}(u_i, c)$, $\bar{\tau}(c, c)$, $\bar{\tau}(\rho, u_i)/\bar{\rho}$, and $\bar{\tau}(\rho, c)$, performed by analyzing the same DNS data.^{39,40} All these results considered jointly encourage further assessment of gradient models as a promising tool for LES research into premixed turbulent combustion. Specifically, the models should be assessed under substantially different conditions by analyzing other DNS data. Moreover, *a posteriori* studies are required, e.g., to explore the problem of numerical stability of these models.

ACKNOWLEDGMENTS

The financial support by Swedish Research Council (grant 2023-04407) is gratefully acknowledged. The authors are very grateful to Professor S. Chaudhuri and Dr. H. Dave for sharing their DNS data.

AUTHOR DECLARATIONS

Conflict of Interest

The authors have no conflicts to disclose.

Author Contributions

Andrei N. Lipatnikov: Conceptualization (equal); Formal analysis (equal); Investigation (equal); Methodology (equal); Validation (equal); Writing – original draft (equal). **Vladimir A. Sabelnikov:** Conceptualization (equal); Formal analysis (equal); Investigation (equal); Methodology (equal); Validation (equal); Writing – original draft (equal).

DATA AVAILABILITY

The data that support the findings of this study are available from the corresponding author upon reasonable request.

REFERENCES

- S. B. Pope, *Turbulent Flows* (Cambridge University Press, Cambridge, UK, 2000).
- C. Meneveau and J. Katz, "Scale-invariance and turbulence models for large-eddy simulation," *Annu. Rev. Fluid Mech.* **32**, 1 (2000).
- M. Lesieur, O. Metais, and P. Comte, *Large-Eddy Simulations of Turbulence* (Cambridge University Press, Cambridge, UK, 2005).
- E. Garnier, N. Adams, and P. Sagaut, *Large Eddy Simulation for Compressible Flows (Scientific Computation)* (Springer, Berlin, 2009).
- J. Janicka and A. Sadiki, "Large eddy simulation of turbulent combustion systems," *Proc. Combust. Inst.* **30**, 537 (2005).
- H. Pitsch, "Large-eddy simulation of turbulent combustion," *Annu. Rev. Fluid Mech.* **38**, 453 (2006).
- C. J. Rutland, "Large-eddy simulations for internal combustion engines - a review," *Int. J. Engine Res.* **12**, 421 (2011).
- L. Y. M. Gicquel, G. Staffelbach, and T. Poinso, "Large eddy simulations of gaseous flames in gas turbine combustion chambers," *Prog. Energy Combust. Sci.* **38**, 782 (2012).
- N. Chakraborty, "Influence of thermal expansion on fluid dynamics of turbulent premixed combustion and its modelling implications," *Flow. Turbul. Combust.* **106**, 753 (2021).
- E. Hawkes and S. R. Cant, "A flame surface density approach to large-eddy simulation of premixed turbulent combustion," *Proc. Combust. Inst.* **28**, 51 (2000).
- I. K. Nwagwe, H. G. Weller, G. R. Tabor, A. D. Gosman, M. Lawes, C. G. W. Sheppard, and R. Woolley, "Measurements and large eddy simulations of turbulent premixed flame kernel growth," *Proc. Combust. Inst.* **28**, 59 (2000).
- O. Colin, F. Ducros, D. Veynante, and T. Poinso, "A thickened flame model for large eddy simulations of turbulent premixed combustion," *Phys. Fluids* **12**, 1843 (2000).
- F. Charlette, C. Meneveau, and D. Veynante, "A power-law flame wrinkling model for LES of premixed turbulent combustion. Part II: Dynamic formulation," *Combust. Flame* **131**, 181 (2002).
- C. Fureby, "A fractal flame-wrinkling large eddy simulation model for premixed turbulent combustion," *Proc. Combust. Inst.* **30**, 593 (2005).
- V. L. Zimont and V. Battaglia, "Joint RANS/LES approach to premixed flame modelling in the context of the TFC combustion model," *Flow. Turbul. Combust.* **77**, 305 (2006).
- V. Molkov, F. Verbecke, and D. Makarov, "LES of hydrogen-air deflagrations in a 78.5 m tunnel," *Combust. Sci. Technol.* **180**, 796 (2008).
- F. Zhang, P. Habisreuther, M. Hettel, and H. Bockhorn, "Modelling of a premixed swirl-stabilized flame using a turbulent flame speed closure model for LES," *Flow. Turbul. Combust.* **82**, 537 (2009).
- B. Fiorina, R. Mercier, G. Kuenne, A. Ketelheun, A. Avdić, J. Janicka, D. Geyer, A. Dreizler, E. Alenius, C. Duwig, P. Trisjono, K. Kleinheinz, S. Kang, H. Pitsch, F. Proch, F. Cavallo Marincola, and A. Kempf, "Challenging modeling strategies for LES of non-adiabatic turbulent stratified combustion," *Combust. Flame* **162**, 4264 (2015).
- S. Zhang and C. J. Rutland, "Premixed flame effects on turbulence and pressure related terms," *Combust. Flame* **102**, 447 (1995).
- J. O'Brien, C. A. Z. Towery, P. E. Hamlington, M. Ihme, A. Y. Poludnenko, and J. Urzay, "The cross-scale physical space transfer of kinetic energy in turbulent premixed flames," *Proc. Combust. Inst.* **36**, 1967 (2017).
- J. Lee, J. F. MacArt, and M. E. Mueller, "Heat release effects on the Reynolds stress budget in turbulent premixed jet flames at low and high Karlovitz numbers," *Combust. Flame* **216**, 1 (2020).
- Y. Su, Z. Lu, and Y. Yang, "Suppression of the turbulent kinetic energy and enhancement of the flame-normal Reynolds stress in premixed jet flames at small Lewis numbers," *Combust. Flame* **246**, 112461 (2022).
- Y. Wang, K. Luo, H. Xiao, T. Jin, J. Xing, and J. Fan, "A novel subgrid-scale stress model considering the influence of combustion on turbulence: A priori and a posteriori assessment," *Phys. Fluids* **36**, 085161 (2024).
- A. N. Lipatnikov and J. Chomiak, "Effects of premixed flames on turbulence and turbulent scalar transport," *Prog. Energy Combust. Sci.* **36**(1), 1 (2010).
- V. A. Sabelnikov and A. N. Lipatnikov, "Recent advances in understanding of thermal expansion effects in premixed turbulent flames," *Annu. Rev. Fluid Mech.* **49**, 91 (2017).
- A. M. Steinberg, P. E. Hamlington, and X. Zhao, "Structure and dynamics of highly turbulent premixed combustion," *Prog. Energy Combust. Sci.* **85**, 100900 (2021).

- ²⁷R. L. Stratonovich, *Topics in the Theory of Random Noise* (Gordon and Breach, New York, 1963), Vol. 1.
- ²⁸M. Germano, "Turbulence: The filtering approach," *J. Fluid Mech.* **238**, 325 (1992).
- ²⁹A. Leonard, "Energy cascade in large-eddy simulations of turbulent fluid flows," *Adv. Geophys.* **18**, A237 (1975).
- ³⁰R. A. Clark, J. H. Ferziger, and W. C. Reynolds, "Evaluation of subgrid scale turbulence models using a fully simulated turbulent flow," *J. Fluid Mech.* **91**(1), 1 (1979).
- ³¹J. Smagorinsky, "General circulation experiments with the primitive equations. I. The basic experiment," *Mon. Weather Rev.* **91**, 99 (1963).
- ³²S. Tullis and R. S. Cant, "Scalar transport modeling in large eddy simulation of turbulent premixed flames," *Proc. Combust. Inst.* **29**, 2097 (2002).
- ³³A. W. Vreman, J. A. van Oijen, L. P. H. de Goeij, and R. J. M. Bastiaans, "Subgrid scale modeling in large-eddy simulation of turbulent combustion using premixed flamelet chemistry," *Flow. Turbul. Combust.* **82**, 511 (2009).
- ³⁴I. Langella, N. Swaminathan, and R. W. Pitz, "Application of unstrained flamelet SGS closure for multi-regime premixed combustion," *Combust. Flame* **173**, 161 (2016).
- ³⁵F. C. C. Galeazzo, B. Savard, H. Wang, E. R. Hawkes, J. H. Chen, and G. C. K. Filho, "Performance assessment of flamelet models in flame-resolved LES of a high Karlovitz methane/air stratified premixed jet flame," *Proc. Combust. Inst.* **37**, 2545 (2019).
- ³⁶F. B. Keil, M. Klein, and N. Chakraborty, "Sub-grid reaction progress variable variance closure in turbulent premixed flames," *Flow. Turbul. Combust.* **106**, 1195 (2021).
- ³⁷Z. Nikolaou, P. Domingo, and L. Vervisch, "Revisiting the modelling framework for the unresolved scalar variance," *J. Fluid Mech.* **983**, A47 (2024).
- ³⁸V. A. Sabelnikov, S. Nishiki, and A. N. Lipatnikov, "A priori assessment of gradient models of joint cumulants for large eddy simulations of premixed turbulent flames," *Phys. Fluids* **37**, 075107 (2025).
- ³⁹H. L. Dave, A. Mohan, and S. Chaudhuri, "Genesis and evolution of premixed flames in turbulence," *Combust. Flame* **196**, 386 (2018).
- ⁴⁰H. L. Dave and S. Chaudhuri, "Evolution of local flame displacement speeds in turbulence," *J. Fluid Mech.* **884**, A46 (2020).
- ⁴¹S. Liu, C. Meneveau, and J. Katz, "On the properties of similarity subgrid-scale models as deduced from measurements in a turbulent jet," *J. Fluid Mech.* **275**, 83 (1994).
- ⁴²A. W. Cook and J. J. Riley, "A subgrid model for equilibrium chemistry in turbulent flows," *Phys. Fluids* **6**, 2868 (1994).
- ⁴³B. Vreman, B. Geurts, and H. Kuerten, "Large eddy simulation of the temporal mixing layer using the Clark model," *Theoret. Comput. Fluid Dyn.* **8**, 309 (1996).
- ⁴⁴J. Réveillon and L. Vervisch, "Response of the dynamic LES model to heat release induced effects," *Phys. Fluids* **8**, 2248 (1996).
- ⁴⁵J. Jiménez, A. Liñán, M. M. Rogers, and F. J. Higuera, "A priori testing of subgrid models for chemically reacting non-premixed turbulent shear flows," *J. Fluid Mech.* **349**, 149 (1997).
- ⁴⁶A. Leonard, "Large-eddy simulation of chaotic convection and beyond," AIAA Paper 97-0204 (1997).
- ⁴⁷A. W. Cook, "Determination of the constant coefficient in scale similarity models of turbulence," *Phys. Fluids* **9**, 1485 (1997).
- ⁴⁸A. W. Cook and J. J. Riley, "Subgrid scale modelling for turbulent flows," *Combust. Flame* **112**, 593 (1998).
- ⁴⁹V. Borue and S. A. Orszag, "Local energy flux and subgrid-scale statistics in three-dimensional turbulence," *J. Fluid Mech.* **366**, 1 (1998).
- ⁵⁰C. D. Pierce and P. Moin, "A dynamic model for subgrid-scale variance and dissipation rate of a conserved scalar," *Phys. Fluids* **10**, 3041 (1998).
- ⁵¹D. Carati, G. S. Winckelmans, and H. Jeanmart, "On the modeling of the subgrid-scale and filtered-scale stress tensors in large-eddy simulation," *J. Fluid Mech.* **441**, 119 (2001).
- ⁵²M. B. Parlange, C. Meneveau, and W. E. Eichinger, "A priori field study of the subgrid-scale heat fluxes and dissipation in the atmospheric surface layer," *J. Atmos. Sci.* **58**, 2673 (2001).
- ⁵³G. S. Winckelmans, A. A. Wray, O. V. Vasilyev, and H. Jeanmart, "Explicit-filtering large-eddy simulations using the tensor-diffusivity model supplemented by a dynamic Smagorinsky term," *Phys. Fluids* **13**, 1385 (2001).
- ⁵⁴B.-C. Wang, E. Yee, D. J. Bergstrom, and O. Iida, "New dynamic subgrid-scale heat flux models for large-eddy simulation of thermal convection based on the general gradient diffusion hypothesis," *J. Fluid Mech.* **604**, 125 (2008).
- ⁵⁵G. D. Portwood, B. T. Nadiga, J. A. Saenz, and D. Livescu, "Interpreting neural network models of residual scalar flux," *J. Fluid Mech.* **907**, A23 (2021).
- ⁵⁶S. T. Salesky, K. Gillis, J. Anderson, I. Helman, W. Cantrell, and R. A. Shaw, "Modeling the subgrid-scale scalar variance: A priori tests and application to supersaturation in cloud turbulence," *J. Atmos. Sci.* **81**, 839 (2024).
- ⁵⁷A. Cimarelli, A. Abba, and M. Germano, "General formalism for a reduced description and modelling of momentum and energy transfer in turbulence," *J. Fluid Mech.* **866**, 865 (2019).
- ⁵⁸L. C. Berselli, T. Iliescu, and W. J. Layton, *Mathematics of Large Eddy Simulation of Turbulent Flows* (Springer, Berlin, 2006).
- ⁵⁹J. Bardina, J. Ferziger, and W. Reynolds, *Improved Turbulence Models Based on Large Eddy Simulation of Homogeneous, Incompressible, Turbulent Flows* (Stanford University, 1983).
- ⁶⁰C. G. Speziale, "Galilean invariance of subgrid-scale stress models in the large-eddy simulation of turbulence," *J. Fluid Mech.* **156**, 55 (1985).
- ⁶¹A. N. Lipatnikov and V. A. Sabelnikov, "An extended flamelet-based presumed probability density function for predicting mean concentrations of various species in premixed turbulent flames," *Int. J. Hydrogen Energy* **45**, 31162 (2020).
- ⁶²A. N. Lipatnikov and V. A. Sabelnikov, "Evaluation of mean species mass fractions in premixed turbulent flames: A DNS study," *Proc. Combust. Inst.* **38**, 6413 (2021).
- ⁶³V. A. Sabelnikov, A. N. Lipatnikov, S. Nishiki, H. L. Dave, F. E. Hernández-Pérez, W. Song, and H. G. Im, "Dissipation and dilatation rates in premixed turbulent flames," *Phys. Fluids* **33**, 035112 (2021).
- ⁶⁴A. N. Lipatnikov and V. A. Sabelnikov, "Flame folding and conditioned concentration profiles in moderately intense turbulence," *Phys. Fluids* **34**, 065119 (2022).
- ⁶⁵A. N. Lipatnikov and V. A. Sabelnikov, "Influence of small-scale turbulence on internal flamelet structure," *Phys. Fluids* **35**, 055128 (2023).
- ⁶⁶A. N. Lipatnikov, "A priori test of perfectly stirred reactor approach to evaluating mean fuel consumption and heat release rates in highly turbulent premixed flames," *Int. J. Engine Res.* **24**, 4034 (2023).
- ⁶⁷A. N. Lipatnikov, V. A. Sabelnikov, and N. V. Nikitin, "Opposite effects of flame-generated potential and solenoidal velocity fluctuations on flame surface area in moderately intense turbulence," *Proc. Combust. Inst.* **40**, 105238 (2024).
- ⁶⁸A. N. Lipatnikov, "A priori assessment of a simple approach to evaluating burning rate in large eddy simulations of premixed turbulent combustion," *Phys. Fluids* **36**, 115152 (2024).
- ⁶⁹N. Babkovskaia, N. E. L. Haugen, and A. Brandenburg, "A high-order public domain code for direct numerical simulations of turbulent combustion," *J. Comput. Phys.* **230**(1), 1 (2011).
- ⁷⁰J. Li, Z. Zhao, A. Kazakov, and F. L. Dryer, "An updated comprehensive kinetic model of hydrogen combustion," *Int. J. Chem. Kinetics* **36**, 566 (2004).
- ⁷¹T. J. Poinsot and S. K. Lele, "Boundary conditions for direct simulations of compressible viscous flows," *J. Comput. Phys.* **101**, 104 (1992).
- ⁷²A. N. Lipatnikov and V. A. Sabelnikov, "Karlovitz numbers and premixed turbulent combustion regimes for complex-chemistry flames," *Energies* **15**, 5840 (2022).
- ⁷³P. F. Huang, G. N. Coleman, and P. Bradshaw, "Compressible turbulent channel flows: DNS results and modelling," *J. Fluid Mech.* **305**, 185 (1995).
- ⁷⁴H. Aluie, S. Li, and H. Li, "Conservative cascade of kinetic energy in compressible turbulence," *Astrophys. J.* **751**, L29 (2012).
- ⁷⁵H. Aluie, "Scale decomposition in compressible turbulence," *Phys. D* **247**, 54 (2013).

- ⁷⁶F. A. Williams, *Combustion Theory*, 2nd ed. (Benjamin/Cummings, Menlo Park, CA, 1985).
- ⁷⁷M. Germano, U. Piomelli, P. Moin, and W. H. Cabot, "A dynamic subgrid-scale eddy viscosity model," *Phys. Fluids* **3**, 1760 (1991).
- ⁷⁸P. Domingo and L. Vervisch, "Recent developments in DNS of turbulent combustion," *Proc. Combust. Inst.* **39**, 2055 (2023).
- ⁷⁹A. Lees and H. Aluie, "Baropycnal work: A mechanism for energy transfer across scales," *Fluids* **4**, 92 (2019).
- ⁸⁰B. Vreman, B. Geurts, and H. Kuerten, "Large-eddy simulation of the turbulent mixing layer," *J. Fluid Mech.* **339**, 357 (1997).
- ⁸¹G. Balarac, J. Le Sommer, X. Meunier, and A. Vollant, "A dynamic regularized gradient model of the subgrid-scale scalar flux for large eddy simulations," *Phys. Fluids* **25**, 075107 (2013).
- ⁸²A. Vollant, G. Balarac, and C. E. Corre, "A dynamic regularized gradient model of the subgrid-scale stress tensor for large-eddy simulation," *Phys. Fluids* **28**, 025114 (2016).
- ⁸³Y. Fabre and G. Balarac, "Development of a new dynamic procedure for the Clark model of the subgrid-scale scalar flux using the concept of optimal estimator," *Phys. Fluids* **23**, 115103 (2011).
- ⁸⁴H. Lu and F. Porté-Agel, "A modulated gradient model for scalar transport in large-eddy simulation of the atmospheric boundary layer," *Phys. Fluids* **25**, 015220 (2013).